[20] Investigation of Protein Motions via Relaxation Measurements

By JEFFREY W. PENG and GERHARD WAGNER

Introduction

The measurement of heteronuclear nuclear magnetic resonance (NMR) relaxation parameters provides a powerful method by which to study the internal dynamics of proteins. In particular, the relaxation properties of protonated heteronuclei such as ^{15}N or $^{13}C^{\alpha}$ are typically dominated by the dipole–dipole interaction with the attached proton(s); therefore, the relaxation data can be interpreted in terms of the motions of the interspin bond vectors. The use of heteronuclear proton-detected NMR pulse techniques for the purpose of relaxation studies has greatly reduced the original problems of measurement, which included inherent low sensitivity of the heteronuclei and poor resolution in one-dimensional (1D) heteronuclear spectra. The sensitivity of the pulse techniques are further augmented by the increasing availability of isotopically enriched protein samples. With current methods, one can measure heteronuclear relaxation parameters for practically each residue in a protein. Thus, the spectroscopist has access to the internal dynamics of many locations within the molecule. The dynamics information gained can then provide additional insight for studies of protein structure and function.

The use of 1D heteronuclear polarization transfer schemes to measure heteronuclear relaxation rates was first developed by Sklenar *et al.*[1] and Kay *et al.*[2] Incorporation of these methods into two-dimensional (2D) heteronuclear correlation spectra was first achieved by Nirmala and Wagner.[3] This facilitated measurement of all $^{13}C^{\alpha}$ T_1 values for basic pancreatic trypsin inhibitor (BPTI) at natural abundance (58 residues, molecular weight 5000), which was the first detailed heteronuclear relaxation study of a protein. A more comprehensive set of ^{15}N relaxation parameters including T_1, T_2, and heteronuclear nuclear Overhauser effects (NOEs) were measured on isotopically enriched staphylococcal nuclease by Kay *et al.*[4] The larger set of relaxation data permitted a more detailed description of the backbone dynamics in terms of the "model-free" formal-

[1] V. Sklenar, D. Torchia, and A. Bax, *J. Magn. Reson.* **73,** 375 (1987).
[2] L. E. Kay, T. Jue, B. Bangerter, and P. C. Demou, *J. Magn. Reson.* **73,** 558 (1987).
[3] N. R. Nirmala and G. Wagner, *J. Am. Chem. Soc.* **110,** 7557 (1988).
[4] L. E. Kay, D. A. Torchia, and A. Bax, *Biochemistry* **28,** 8972 (1989).

METHODS IN ENZYMOLOGY, VOL. 239

ism of Lipari and Szabo.[5,6] Since then, the number of heteronuclear relaxation studies of proteins has been steadily increasing. ^{13}C studies include C^{α} studies on the Xfin zinc finger and leucine methyl carbon studies of staphylococcal nuclease.[7,8] ^{15}N studies include those on interleukin 1β,[9] calbindin D9k,[10] ubiquitin,[11] glucose permease,[12] calmodulin,[13] eglin c,[14] ribonuclease H,[15] interleukin 4,[16] and thioredoxin.[17] Thus far, protein ^{13}C relaxation studies have been less numerous owing to the higher cost of ^{13}C labeling and complications expected from homonuclear ^{13}C–^{13}C scalar coupling effects in uniformly enriched samples. Consequently, ^{13}C relaxation studies have been done at natural abundance with high concentration samples or on molecules that have selective labels.

This chapter focuses on the 2D pulse sequences applicable for measuring relaxation rates in singly protonated heteronuclear spin systems, such as ^{15}N–^{1}H and $^{13}C^{\alpha}$–^{1}H. We shall use the symbols I and S to denote the operators or expectation values of the proton and heterospin, respectively. The Cartesian product operator basis of Sørensen *et al.* will describe the general state of the spin system.[18] Additionally, we more often refer to the relaxation of a given spin order. Spin order simply refers to a macroscopic spin state, and it can be identified as the ensemble-averaged expectation value of a particular product operator. Spin order encompasses the familiar longitudinal magnetization and transverse magnetization, as well as antiphase transverse magnetizations, longitudinal two-spin order, and multiple (e.g., zero and double) quantum coherences. No attempt is made here to provide an in-depth review of the theory of nuclear spin relaxation. Instead, we refer the reader to excellent theoretical reviews in the literature.[19–22]

In what follows, we first briefly recapitulate how molecular dynamics information is transmitted to the heteronuclear relaxation rates. We then survey the various auto- and cross-relaxation processes to consider in an IS spin system. This is followed by a description of a number of relaxation pulse sequences and a general outline of data acquisition and analysis procedures used in our laboratory. Finally, brief mention is made of the work in measuring relaxation parameters for non-IS spin systems, which include side-chain ^{13}C relaxation measurements and selective proton relaxation measurements.

General Considerations of Heteronuclear Relaxation

Relaxation Mechanisms and Molecular Motion

It is useful to review the connection between molecular motion and the heteronuclear NMR relaxation parameters. Motions of the IS bonds with respect to the external magnetic field, $\mathbf{B}_0$, creates local fluctuating fields at the I and S nuclei. The interaction between the I and S magnetic moments and these local fields provides the means whereby a perturbed IS spin system can relax back to equilibrium. In theoretical treatments, these interactions are expressed as perturbing Hamiltonians that couple the spin degrees of freedom with those of molecular motion (the lattice).

The relaxation behavior of the heteronuclear S spin is principally controlled by two interactions: the heteronuclear dipole–dipole (DD) interaction and the S spin chemical shift anisotropy (CSA). In the DD interaction, the S spins experience the local dipolar field of the directly bonded I spin. The IS bond dynamics cause the local field to fluctuate, and this encourages relaxation. In the CSA interaction, relaxation is caused by fluctuations in the local shielding of the S spin. The CSA interaction actually reflects the motions of the principal axes of S spin shielding tensor with respect to $\mathbf{B}_0$. However, previous studies have indicated that the tensor is approximately

[5] G. Lipari and A. Szabo, *J. Am. Chem. Soc.* **104,** 4546 (1982a).
[6] G. Lipari and A. Szabo, *J. Am. Chem. Soc.* **104,** 4559 (1982b).
[7] A. G. Palmer III, M. Rance, and P. E. Wright, *J. Am. Chem. Soc.* **113,** 4371 (1991).
[8] L. K. Nicholson, L. E. Kay, D. M. Baldisseri, J. Arango, P. E. Young, A. Bax, and D. A. Torchia, *Biochemistry* **31,** 5253 (1992).
[9] G. M. Clore, P. C. Driscoll, P. T. Wingfield, and A. M. Gronenborn, *Biochemistry* **29,** 7387 (1990).
[10] J. Kördel, N. J. Skelton, M. Akke, A. G. Palmer III, and W. J. Chazin, *Biochemistry* **31,** 4856 (1992).
[11] D. M. Schneider, M. J. Dellwo, and A. J. Wand, *Biochemistry* **31,** 2464 (1992).
[12] M. J. Stone, W. J. Fairbrother, A. G. Palmer III, J. Reizer, M. H. Saier, and P. E. Wright, *Biochemistry* **31,** 5253 (1992).
[13] G. Barbato, M. Ikura, L. E. Kay, R. W. Pastor, and A. Bax, *Biochemistry* **31,** 5269 (1992).
[14] J. W. Peng and G. Wagner, *Biochemistry* **31,** 8571 (1992).
[15] R. Powers, G. M. Clore, S. J. Stahl, P. T. Wingfield, and A. M. Gronenborn, *Biochemistry* **31,** 9150 (1992).
[16] C. Redfield, J. Boyd, L. J. Smith, A. R. G. Smith, and C. M. Dobson, *Biochemistry* **31,** 10431 (1992).
[17] M. J. Stone, K. Chandrasekhar, A. Holmgren, P. E. Wright, and H. J. Dyson, *Biochemistry* **32,** 426 (1993).
[18] O. W. Sørensen, M. H. Eich, M. H. Levitt, G. Bodenhausen, and R. R. Ernst, *Prog. NMR Spectrosc.* **16,** 163 (1983).
[19] A. G. Redfield, *Adv. Magn. Reson.* **1,** 1 (1965).
[20] A. D. Bain and R. M. Lynden-Bell, *Mol. Phys.* **2,** 325 (1975).
[21] L. G. Werbelow and D. M. Grant, *Adv. Magn. Reson.* **9,** 189 (1977).
[22] R. R. Vold and R. R. Vold, *Prog. NMR Spectrosc.* **12,** 79 (1978).

axially symmetric.[23,24] If the symmetry axis bears a fixed orientation with respect to the *IS* bond in the molecular frame, then the motions of the tensor symmetry axis are essentially the same as those of the *IS* bond. Thus, in both interactions, the *IS* bond motions power the local fields responsible for *S* spin relaxation. Note that DD interactions between the *S* spin and more distant nonbonded protons are negligible owing to the inverse sixth power dependence of the DD interaction on the interspin distance.[25] Therefore, the *S* spin relaxation properties can be interpreted exclusively in the context of the *IS* bond dynamics.

The relaxation behavior of the proton *I* spins are more complex since both heteronuclear and homonuclear DD relaxation processes have to be considered. The proton homonuclear DD interaction will tend to couple the relaxation of the *I* spin to a larger network of proton–proton auto- and cross-relaxation pathways. To illustrate, the amide proton of an ^{15}N–^{1}H spin system will be relaxed by both the bonded ^{15}N nucleus and other protons within approximately 5 Å distance. This has important consequences for experiments aimed at measuring the relaxation rates of two-spin product operators such as $2I_zS_z$ and $2I_zS_x$. Thus, in general, we expect that the relaxation rates of spin orders involving the proton *I* spin will depend not only on the *IS* bond dynamics but also on the dynamics of other distinct proton–proton spin pairs.

Relaxation Rates and Spectral Density Functions

In more quantitative terms, the dependence of the heteronuclear relaxation rates on the *IS* bond dynamics can be expressed as a dependence on the so-called power spectral density functions, $J(\omega)$. Each *IS* bond has a specific $J(\omega)$ that characterizes the *IS* bond dynamics (see, e.g., Wittebort and Szabo[26]). Thus, the elucidation of $J(\omega)$ is the central aim of molecular dynamics studies using heteronuclear relaxation measurements. In essence, the $J(\omega)$ are frequency distribution functions that profile the frequency content of *IS* bond motions. In heteronuclear studies, the *IS* bond length is essentially fixed, and, therefore, the bond motions refer to rotational fluctuations with respect to $\mathbf{B}_0$. The width of $J(\omega)$ is related to the time scale of the *IS* bond fluctuations. Those *IS* bonds

[23] Y. Hiyama, C. Niu, J. V. Silverton, A. Bavaso, and D. A. Torchia, *J. Am. Chem. Soc.* **110,** 2378 (1988).
[24] A. Shoji, T. Ozaki, T. Fujito, K. Deguchi, S. Ando, and I. Ando, *J. Am. Chem. Soc.* **112,** 4693 (1990).
[25] A. Allerhand, D. Doddrell, V. Glushko, D. W. Cochran, E. Wenkert, P. J. Lawson, and F. R. N. Gurd, *J. Am. Chem. Soc.* **93,** 544 (1971).
[26] R. J. Wittebort and A. Szabo, *J. Chem. Phys.* **69,** 1723 (1978).

that experience more rapid reorientation are expected to have a wider distribution of frequencies in $J(\omega)$ than those experiencing slower reorientation. In contrast, the total area under the $J(\omega)$ function is independent of any time scale and is related to the mean squared amplitude of the rotational fluctuations. Because this is a constant over the ensemble of molecules tumbling in solution, the area under $J(\omega)$ is the same for all *IS* bonds.[27]

For a given *IS* bond, the heteronuclear relaxation rates consist of weighted sums of $J(\omega)$, evaluated at specific frequencies. The general form is given by

$$R_{\text{spins}}(Q) = \sum_{i=1}^{5} c_i J(\omega_i) + (\text{pure proton DD relaxation terms}) \quad (1)$$

We use the nomenclature $R_{\text{spins}}(Q)$, where the subscript spins denotes the relevant spins involved in the relaxation, and Q is the particular spin operator enjoying the relaxation.[28] The summation runs over the five sampling frequencies 0, ω_S, ω_I, and $\omega_S \pm \omega_I$, and the coefficients c_i are the appropriate weights. These c_i are the squares of the "instantaneous Larmor frequencies" associated with the Hamiltonians describing the heteronuclear DD and *S* spin CSA interactions. The pure proton terms reflect the possible dependence of the relaxation rate on homonuclear proton dipole–dipole interactions. These pure proton terms contain different spectral density functions, $J_{IA^i}(\omega)$, that describe the fluctuations of interspin vectors connecting two proton nuclei *I* and A^i, and are not to be confused with $J(\omega)$, which strictly describes *IS* bonds. A^i refers to the *i*th proton close in space to proton *I* (within ~5 Å) that is not bonded to the same heterospin *S*; note that there could be several such protons, and hence the superscript *i* is used. Equation (1) reveals that the efficiency of relaxation depends on the extent of overlap between the $J(\omega)$ distribution and the sharp frequencies, ω, selected by the spin system and the applied field, $\mathbf{B}_0$. Thus, finer mappings of $J(\omega)$ require heteronuclear relaxation measurements at multiple fields.

Kinetics of IS Spin System Relaxation

For an *IS* spin system there are potentially 15 nontrivial spin orders whose relaxation properties can be studied to gain dynamics information. These include $\langle I_z \rangle$, $\langle S_z \rangle$, $\langle 2I_zS_z \rangle$, $\langle I_x \rangle$, $\langle S_x \rangle$, $\langle I_y \rangle$, $\langle S_y \rangle$, $\langle 2I_zS_x \rangle$, $\langle 2I_zS_y \rangle$,

[27] A. Abragam, "The Principles of Nuclear Magnetism." Oxford Univ. Press (Clarendon), 1961.
[28] J. W. Peng and G. Wagner, *J. Magn. Reson.* **82,** 308 (1992).

$\langle 2I_xS_z\rangle$, $\langle 2I_yS_z\rangle$, $\langle 2I_xS_x\rangle$, $\langle 2I_yS_y\rangle$, $\langle 2I_xS_y\rangle$, and $\langle 2I_yS_x\rangle$. In the ideal situation, perturbation of any one these spin orders would be followed by a simple single exponential recovery toward equilibrium. Unfortunately, the existence of cross-relaxation can destroy this ideality by coupling the relaxation time courses of various spin orders together. The summary kinetics of these spin orders under the dual presence of auto- and cross-relaxation are described by a system of first-order linear coupled differential equations given by

$$\frac{d\langle \mathbf{Q}\rangle}{dt} = -\mathbf{R}\langle \mathbf{Q}\rangle \tag{2}$$

In Eq. (2), $\langle \mathbf{Q}\rangle$ is a vector of spin orders obtained by taking the trace of the associated spin operators with the density operator $\sigma(t)$. $\mathbf{R}$ is the matrix representation of the relaxation superoperator. The diagonal elements are the autorelaxation rates, and the off-diagonal elements represent cross-relaxation rates. Methods for the computation of auto- and cross-relaxation rates directly from the relaxation superoperator are given in the literature.[19–22]

Tables I and II list autorelaxation rates and cross-relaxation rates for an IS spin system. In formulating Tables I and II, we have considered only the heteronuclear DD interaction, the S spin CSA, and proton–proton DD interactions. The particular auto- or cross-relaxation rate is identified in the left-hand column. Other columns contain the c_i weighting coefficients in the expression for $R_{\text{spins}}(Q)$ given in Eq. (1). The c_i coefficients include the constants d, c, and K which are given in terms of various physical constants denoted in the footnotes to Tables I and II. The constant d pertains to DD relaxation effects, and the constant c pertains to CSA relaxation effects. K is concerned with CSA–DD cross-correlation effects (see below). Ω_S and Δ_S are the Larmor frequency and chemical shift anisotropy for the S spin, respectively; r_{IS} is the interspin distance between the I and S nuclei; γ_I and γ_S are the gyromagnetic ratios for the I and S spins, respectively. In Table I, potential contributions from pure proton DD longitudinal or transverse relaxation are denoted by nonzero entries under the ρ_L and ρ_T columns, respectively. In Table II, nonzero entries under σ_L^i and σ_T^i signify proton DD longitudinal or transverse cross-relaxation, respectively, between proton I and another distinct proton A^i.

To get a rate expression, one first multiplies the weighting coefficients listed in the columns in Tables I and II with the quantities in the column headings and then adds the resultant products [as per Eq. (1)]. It is understood that the product operators related by a simple rotation about the laboratory z axis (about the direction of $\mathbf{B}_0$) have the same relaxation rates. Note that the proton homonuclear rates ρ_L, ρ_T, σ_L^i, and σ_T^i are

TABLE I
IS SPIN SYSTEM AUTORELAXATION RATES

Autorelaxation[a,b]	$J(0)$	$J(\omega_S)$	$J(\omega_I - \omega_S)$	$J(\omega_I)$	$J(\omega_I + \omega_S)$	ρ_L	ρ_T
Single-quantum heteronucleus							
$R_1(S_z)$	0	$3d + c$	d	0	$6d$	0	0
$R_2(S_x)$	$2d + (2c/3)$	$(3d + c)/2$	$d/2$	$3d$	$3d$	0	0
Single-quantum proton							
$R_1(I_z)$	0	0	d	$3d$	$6d$	1	0
$R_2(I_x)$	$2d$	$3d$	$d/2$	$3d/2$	$3d$	0	1
Longitudinal two-spin order							
$R_{IS}(2I_zS_z)$	0	$3d + c$	0	$3d$	0	1	0
Single-quantum antiphase coherence							
$R_{IS}(2I_zS_x)$	$2d + (2c/3)$	$(3d + c)/2$	$d/2$	0	$3d$	1	0
$R_{IS}(2I_xS_z)$	$2d$	c	$d/2$	$3d/2$	$3d$	0	1
Pure double-quantum coherence							
$R_{IS}(2I_1S_1)$	$2c/3$	$(3d + c)/2$	0	$3d/2$	$6d$	0	1
Pure difference-quantum coherence							
$R_{IS}(2I_1S_{-1})$	$2c/3$	$(3d + c)/2$	d	$3d/2$	0	0	1

[a] Autorelaxation rate = $[\Sigma_i^{\text{cols}}(\text{weight})_i\ J(\omega_i)] + (\text{weight } \rho_L)\rho_L + (\text{weight } \rho_T)\rho_T$.
[b] Constants are $d = \hbar^2\gamma_I^2\gamma_S^2/4r_{IS}^6$, $c = \Omega_S^2\Delta_S^2/3$, and expressions are in cgs units.

TABLE II
IS SPIN SYSTEM CROSS-RELAXATION RATES

Cross-relaxation[a,b]	$J(0)$	$J(\omega_S)$	$J(\omega_I - \omega_S)$	$J(\omega_I)$	$J(\omega_I + \omega_S)$	σ^i_L	σ^i_T
Heteronuclear dipolar cross-relaxation							
$R_S(I_z \leftrightarrow S_z)$	0	0	$-d$	0	$6d$	0	0
Proton longitudinal cross-relaxation (NOE)[c]							
$R_I(I_z \leftrightarrow A^i_z)$	0	0	0	0	0	1	0
Proton transverse cross-relaxation (ROE)[c]							
$R_I(I_x \leftrightarrow A^i_x)$	0	0	0	0	0	0	1
CSA–dipolar cross-correlated cross-relaxation							
$R_S(S_z \leftrightarrow 2I_zS_z)$	0	K	0	0	0	0	0
$R_S(S_x \leftrightarrow 2I_zS_x)$	$2K/3$	$K/2$	0	0	0	0	0

[a] Constants are $d = \hbar^2\gamma_I^2\gamma_S^2/4r_{IS}^6$, $c = \Omega_S^2\Delta_S^2/3$, and $K = \hbar\gamma_I\gamma_S\Omega_S\Delta_S\langle P_2(\cos\Phi)\rangle/r_{IS}^3$, and expressions are in cgs units.

[b] Cross-rate = $[\Sigma_i^{\text{cols}}(\text{weight})_i J(\omega_i)]$ + (weight σ^i_L)σ^i_L + (weight σ^i_T)σ^i_T.

[c] $\sigma^i_L = (\hbar^2\gamma_I^4/4r_{IA^i}^6)\{6J_{IA^i}(2\omega_I) - J_{IA^i}(0)\}$. $\sigma^i_T = (\hbar^2\gamma_I^4/4r_{IA^i}^6)\{2J_{IA^i}(0) + 3J_{IA^i}(\omega_I)\}$.

those presented in the literature on laboratory-frame (NOESY) and rotating-frame NOE spectroscopy (ROESY).[29,30] In terms of the aforementioned spectral densities $J_{IA^i}(\omega)$, these rates can be written as

$$\rho_L = \sum_{i=1}^{N} \frac{\hbar^2\gamma_I^4}{4r_{IA^i}^6}\left[J_{IA^i}(0) + 3J_{IA^i}(\omega_I) + 6J_{IA^i}(2\omega_I)\right] \tag{3a}$$

$$\rho_T = \sum_{i=1}^{N} \frac{\hbar^2\gamma_I^4}{4r_{IA^i}^6}\left[(5/2)J_{IA^i}(0) + (9/2)J_{IA^i}(\omega_I) + 3J_{IA^i}(2\omega_I)\right] \tag{3b}$$

$$\sigma^i_L = \frac{\hbar^2\gamma_I^4}{4r_{IA^i}^6}[6J_{IA^i}(2\omega_I) - J_{IA^i}(0)] \tag{3c}$$

$$\sigma^i_T = \frac{\hbar^2\gamma_I^4}{4r_{IA^i}^6}[2J_{IA^i}(0) + 3J_{IA^i}(\omega_I)] \tag{3d}$$

In these formulas, we have approximated $\omega_{A^i} \approx \omega_I$. In the slow tumbling limit where $J_{IA^i}(0)$ dominates the auto- and cross-relaxation rates, the ROE/NOE ratio, σ^i_T/σ^i_L, approaches -2. The superscript i emphasizes the fact that the cross-relaxation rate is governed by specific proton–proton DD interactions defined by the interspin vector r_{IA^i}. In contrast, ρ_L and ρ_T contain the contributions of many proton–proton DD interactions.

[29] S. Macura and R. R. Ernst, *Mol. Phys.* **41,** 95 (1980).
[30] A. A. Bothner-By, R. L. Stephens, J. Lee, C. D. Warren, and R. W. Jeanloz, *J. Am. Chem. Soc.* **196,** 811 (1984).

Table III lists various values for the CSA c constants at different spectrometer field strengths. The ratios of the c constants to the DD d constants are also given. The DD constants, d, are field independent, whereas CSA factors c increase with $\mathbf{B}_0$. Using typical values for the NH and CH bond distances (e.g., 1.02 Å for NH, 1.09 Å for CH) $d \approx 1.30 \times 10^9$ (rad/sec)^2 for ^{15}N systems, and $d \approx 5.37 \times 10^9$ (rad/sec)^2 for ^{13}C systems. A value of -160 ppm is assumed for amide ^{15}N CSA, whereas a value of 25 ppm is used for methine ^{13}C CSA.[7,23] At the highest field of 17.62 T, the CSA factor dominates the DD factor for ^{15}N relaxation. However, the CSA factor is still only about 5% of the DD factor for a ^{13}C. Thus, sole consideration of the DD mechanism for ^{13}C relaxation studies is a well-justified approximation.

The relaxation rates of the single-spin spin orders such as $\langle S_x\rangle$, $\langle S_y\rangle$, and $\langle S_z\rangle$ are quite familiar. Perhaps less familiar are the two-spin relaxation rates. These rates have an explicit dependence on either longitudinal proton DD relaxation signified by ρ_L or transverse proton DD relaxation signified by ρ_T. As a consequence, these spin orders can relax significantly faster than the one-spin counterparts. Furthermore, we note that the double-transverse spin orders such as $\langle 2I_xS_x\rangle$ are really superpositions of pure heteronuclear zero-quantum coherence ($2I_1S_{-1}$) and double-quantum coherence ($2I_1S_1$). It follows that these spin orders relax at the average rate, $R_{IS}(2I_xS_x) = (1/2)[R_{IS}(2I_1S_1) + R_{IS}(2I_1S_{-1})]$. A distinguishing feature of this average rate is that it depends on $J(0)$ only through the CSA. Recall from Table III that the CSA contribution for ^{13}C relaxation is

TABLE III
CHEMICAL SHIFT ANISOTROPY RELAXATION CONSTANTS VERSUS FIELD STRENGTH

Field strength		^{15}N–^{1}H[a]		^{13}C–^{1}H[b]	
^{1}H Frequency (MHz)	$\|\mathbf{B}_0\|$ (tesla)	c ($\times 10^9$ rad/sec)^2	c/d	c ($\times 10^9$ rad/sec)^2	c/d
300	7.04	0.31	0.24	0.05	0.01
400	9.39	0.55	0.42	0.08	0.01
500	11.74	0.87	0.67	0.13	0.02
600	14.09	1.25	0.96	0.19	0.04
750	17.62	1.95	1.50	0.29	0.05

[a] Uses a value of -160 ppm for ^{15}N CSA [Y. Hiyama, C. Niu, J. V. Silverton, A. Bavaso, and D. A. Torchia, *J. Am. Chem. Soc.* **110,** 2378 (1988)]. The ratio c/d is dimensionless. The ^{15}N–^{1}H dipolar constant d is 1.30×10^9 (rad/sec)^2 using a internuclear distance of 1.02 Å.

[b] Uses a value of 25 ppm for ^{13}C CSA [A. G. Palmer III, M. Rance, and P. E. Wright, *J. Am. Chem. Soc.* **113,** 4371 (1991)]. The ratio c/d is dimensionless. The ^{13}C–^{1}H dipolar constant d is 5.37×10^9 (rad/sec)^2 using an internuclear distance of 1.09 Å.

quite small, and therefore $R_{IS}(2I_xS_x)$ essentially lacks a heteronuclear $J(0)$ dependence. Thus, when considering $^{13}C-^{1}H$ relaxation in large proteins at high field, the main contribution to $R_{IS}(2I_xS_x)$ are the $J_{IA^i}(0)$ terms in ρ_T. If this contribution is less than the heteronuclear DD contribution to $J(0)$, then $R_{IS}(2I_xS_x)$ can actually be less than the single-quantum $R_S(S_x)$ value. Generally, the significance of the ρ_T contribution has to be evaluated on the basis of the number of nearby protons, as well as the length and dynamics of associated interproton vectors $\mathbf{r}_{IA}$.

It is useful to identify the cross-relaxation processes one has to consider in the measurement of *IS* relaxation rates. The first process is heteronuclear cross-relaxation mediated by the heteronuclear DD interaction. This has the effect of transferring perturbations experienced by the proton longitudinal magnetization (I_z) to the heterospin longitudinal magnetization (S_z) and vice versa. There are also the effects of homonuclear proton cross-relaxation to consider. Such cross-relaxation promotes magnetization transfers of the type observed in conventional NOESY and ROESY spectra.[29,30] It is to be understood that observation of transverse cross-relaxation relies on the suppression of the differential chemical shift precession rates of the cross-relaxing spins; the ROESY experiment achieves this by means of a spin-lock field. ROESY and NOESY type transfers obviously affect the relaxation behavior of proton one-spin terms such as $\langle I_x\rangle$ and $\langle I_z\rangle$, and this is shown in Table II. However, it should be mentioned that they can also affect the relaxation of the two-spin bilinear spin orders, such as $\langle 2I_zS_z\rangle$, $\langle 2I_zS_x\rangle$, $\langle 2I_xS_z\rangle$, and multiple-quantum spin orders, such as $\langle 2I_xS_x\rangle$. Analogous to the one-spin cases, these two-spin spin orders can cross-relax with other two-spin spin orders of the type $\langle 2A^i_zS_{z,x}\rangle$ and $\langle 2A^i_xS_{z,x}\rangle$. Because the $\langle 2A^i_zS_{z,x}\rangle$ and $\langle 2A^i_xS_{z,x}\rangle$ spin orders involve nuclei that are essentially uncoupled, they cannot be refocused for direct detection.

A more subtle form of cross-relaxation arises from cross-correlation effects. Cross-correlation effects are expected when a spin multiplet is subject to multiple relaxation mechanisms whose local fields (1) perturb the multiplet with different symmetry properties and (2) fluctuate in a correlated manner. The effect is that multiplet members sense local fields of different strengths and therefore relax at different rates. This causes apparent cross-relaxation between spin orders of different rank (e.g., one-spin spin order transfer to two- or three-spin spin order). Here, one must consider the effects of cross-correlation between the heteronuclear DD interaction and the axially symmetric part of the *S* spin CSA. The local fields from these interactions fluctuate in a correlated manner such that the two *S* doublet members experience local fields of different magnitudes. The two doublet members are illustrated in the schematic "spectrum" of

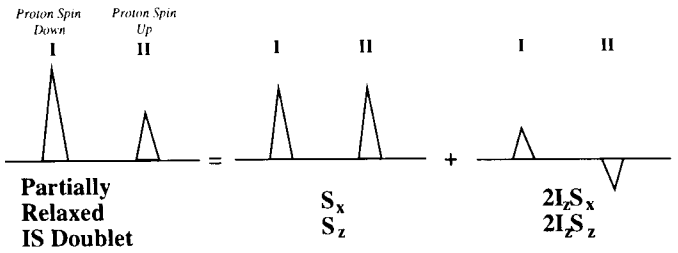

FIG. 1. Schematic decomposition of the partially relaxed, weakly coupled *IS* doublet in terms of one- and two-spin operator products. Local fields arising from the heteronuclear DD and *S* spin CSA relax the *S* spin transitions. The transition with the proton spin up (transition II) senses a stronger net local field than the transition with proton spin down (transition I) and therefore relaxes faster. This is essentially the CSA–DD cross-correlation effect. Differential relaxation of doublet members caused by CSA–DD cross-correlation can be described as cross-relaxation between one- and two-spin order.

Fig. 1. The doublet member with proton spin up (peak II) experiences a slightly augmented local field, whereas the doublet member with proton spin down (peak I) sees a slightly retarded field. Consequently, the doublet members relax at different rates, permitting cross-relaxation transfers such as $\langle S_x\rangle, \leftrightarrow \langle 2I_zS_x\rangle$ and $\langle S_z\rangle \leftrightarrow \langle 2I_zS_z\rangle$.[31–34] In Table II, the factor K scales the cross-correlated cross-relaxation and contains a second-order Legendre polynomial, $\langle P_2[\cos(\Phi)]\rangle$. Here, Φ is the angle between the CSA tensor symmetry axis and the *IS* interspin vector; a value of approximately 20° has been reported for $^{15}N-^{1}H$ spin systems.[23]

Note that all of these cross-relaxation transfers can injure attempts to determine autorelaxation rates by fitting peak intensities to single exponential decays. Because the actual decay will be multiexponential, fitting to a single exponential will introduce some systematic error to the rates. In such cases, it is desirable to tailor the pulse sequences to purge the undesired cross-relaxation effects. It should be noted, however, that cross-relaxation processes are not always deleterious to the experimental results. They are beneficial in that they potentially offer further dynamics information. An example is measurement of the heteronuclear NOE, which probes for the heteronuclear cross-relaxation rate $R_{IS}(S_z \leftrightarrow I_z)$. Additionally, measurements of cross-relaxation rates facilitated by the CSA–DD cross-

[31] M. Goldman, *J. Magn. Reson.* **60,** 437 (1984).
[32] J. Boyd, U. Hommel, and I. D. Campbell, *Chem. Phys. Lett.* **175,** 477 (1990).
[33] A. G. Palmer III, N. J. Skelton, W. J. Chazin, P. E. Wright, and M. Rance, *Mol. Phys.* **75,** 699 (1992).
[34] L. E. Kay, L. K. Nicholson, F. Delaglio, A. Bax, and D. A. Torchia, *J. Magn. Reson.* **97,** 359 (1992).

correlation or by scalar coupling–isotropic chemical shift cross-correlation have been used by Brüschweiler and Ernst to elicit dynamics information.[35]

It should be noted that the proton I spin also has a CSA, which should therefore influence the relaxation through a $J_I^{CSA}(\omega)$ term, which is the spectral density function describing the fluctuations of the proton CSA tensor symmetry axis with respect to $\mathbf{B}_0$. For proton longitudinal relaxation the CSA contribution enters with a $J_I^{CSA}(\omega_I)$ dependence, and for proton transverse relaxation the CSA contribution enters with both $J_I^{CSA}(0)$ and $J_I^{CSA}(\omega_I)$. However, the proton CSA value is rather small, approximately -9 ppm.[36] Also, the value of $J_I^{CSA}(\omega_I)$ is expected to be small for proteins in high field spectrometers. Together, these considerations make the CSA contribution to the proton autorelaxation rates rather minor. Furthermore, potential cross-correlation effects between DD interactions involving the I proton and the I proton CSA are expected to be minor for the essentially the same reasons.

Finally, it should be mentioned that cross-correlations between distinct pairs of DD interactions involving a common I spin can also lead to cross-relaxation. For example, in the case of ^{15}N–^1H systems, the amide proton enjoys DD interactions with both the bonded ^{15}N and other protons close in space. Cross-correlation of these distinct dipolar fields can cause cross-relaxation between $\langle I_z \rangle$ and longitudinal three-spin spin order, as well as between $\langle I_x \rangle$ and doubly antiphase I coherence. These effects tend to be small for proteins in high-field spectrometers for the same reasons that the proton CSA contribution to the proton auto-relaxation rates are small. Sensitive detection of these dipolar cross-correlation effects can be achieved in the rotating frame via selective nuclear spin-locking shared between the correlated interactions.[36,37]

Characterization of $J(\omega)$ Via Relaxation Measurements

Table I reveals that the autorelaxation rates depend on five evaluations of the IS spectral density functions: $J(0)$, $J(\omega_S)$, $J(\omega_I - \omega_S)$, $J(\omega_I)$, and $J(\omega_S)$. Additionally, there is a possible dependence on the I proton longitudinal and transverse relaxation rates, signified by ρ_L or ρ_T. Thus, to determine the spectral density values, one must perform at least six independent relaxation measurements. Usually only three parameters are measured, such as the heteronuclear T_1, T_2, and the NOE. As this is not sufficient to map $J(\omega)$, one adopts models about the motion of the IS

[35] R. Brüschweiler and R. R. Ernst, *J. Chem. Phys.* **96,** 1758 (1992).
[36] I. Burghardt, R. Konrat, and G. Bodenhausen, *Mol. Phys.* **75,** 467 (1992).
[37] T. E. Bull, *J. Magn. Reson.* **93,** 596 (1991).

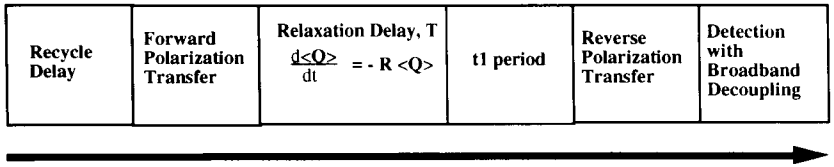

FIG. 2. Organizational scheme for the skeletal 2D proton-detected relaxation experiment. Time increases to the right. The final spectrum is a 2D heteronuclear correlation map with cross-peak intensities dependent on the type and extent of relaxation allowed during the delay T.

bond, such as the "wobbling in a cone" model.[38–40] Dynamic parameters defined by the model are adjusted such that the experimental parameters are best reproduced. Alternatively, "model-free" approaches can be used which do not invoke a mechanistic model of the motion but assume that the autocorrelation function is a sum of exponentials.[5,6] As a consequence, the spectral density function is a sum of Lorentzians centered at $\omega = 0$. The model-free approach of Lipari and Szabo[5,6] has been the most popular method of interpreting relaxation data.

A strategy has been developed to map spectral density functions independent of mechanistic models or models about the time dependence of the autocorrelation function.[14,28] This requires measurements of six independent relaxation parameters: $R_S(S_z)$, $R_S(S_x)$, $R_{IS}(2I_zS_x)$, $R_{IS}(2I_zS_z)$, $R_S(I_z \leftrightarrow S_z)$, and $R_I(I_z)$. The main challenge of this method is that pure autorelaxation and cross-relaxation rates need to be obtained. Therefore, it is important to use pulse sequences that minimize artifacts stemming from undesired coherent and incoherent magnetization transfer processes. It remains to be seen whether this approach has the sensitivity to provide additional insight into aspects of protein internal motions.

Pulse Sequences for Measuring Auto- and Cross-Relaxation Rates in *IS* Spin Systems

General Aspects

Extraction of relaxation rates involves recording a series of 2D spectra using pulse sequences based on a proton-detected 2D heteronuclear shift correlation spectrum. Figure 2 illustrates the basic organization of the

[38] D. E. Woessner, *J. Chem. Phys.* **36,** 1 (1962).
[39] K. Kinoshita, S. Kawato, Jr., and A. Ikegami, *Biophys. J.* **20,** 289 (1977).
[40] R. Richarz, K. Nagayama, and K. Wüthrich, *Biochemistry* **19,** 5189 (1980).

sequences. After a suitably long recycle delay, a polarization transfer based on the INEPT (insensitive nuclei enhanced by polarization transfer) or DEPT (distortionless enhancement by polarization transfer) schemes creates the initial heteronuclear spin order.[41,42] The nonequilibrium spin order experiences auto- and cross-relaxation during the following relaxation delay, which lasts for a duration T. The influences of chemical exchange are also felt during this period. Afterward, the residual spin order is frequency labeled with the chemical shift frequency of the heteronucleus during the t_1 period. Sign discrimination in t_1 can be achieved with the appropriate time-proportional phase incrementation (TPPI) modulation of Marion and Wüthrich.[43] The residual spin order returns to the proton via a second polarization transfer scheme that operates in a reverse sense from the initial one. The sequence concludes with proton acquisition, typically in the presence of heteronuclear broadband decoupling; such as GARP (globally optimized alternating-phase rectangular pulses) or WALTZ-16 (wideband alternating-phase low power technique for zero-residual splitting).[44,45] Because the sequence begins with proton polarization, the length of the recycle delay is adjusted for sufficient proton T_1 relaxation. Short recycle delays will penalize the sensitivity of the experiment and therefore, possibly, the precision of the relaxation rates obtained. However, no systematic errors should be introduced. The final 2D spectrum used for analysis is the heteronuclear correlation map with each cross-peak identifying a particular IS spin system in the protein. The cross-peak intensities have a time dependence dictated by the relaxation kinetics of the IS operators in the relaxation delay T.

Pulse Sequences

We now turn to a more in-depth discussion of several relaxation pulse sequences, which measure both one- and two-spin relaxation rates. Except for the heteronuclear NOE pulse sequence (see below), all pulse sequences involve fitting 2D cross-peak intensities to a single-exponential decay in order to extract an autorelaxation rate. The accuracy of this procedure hinges on the appropriate suppression of cross-relaxation pathways, which would otherwise cause multiexponential relaxation. Therefore, attention will be given to the effects and suppression of cross-relaxation processes in the experiments. Pulse sequences are illustrated starting with Fig. 3A. Further details can be found in the original literature.[1-4]

[41] G. A. Morris and R. Freeman, *J. Am. Chem. Soc.* **101,** 760 (1979).
[42] D. M. Doddrell, D. T. Pegg, and M. R. Bendall, *J. Magn. Reson.* **48,** 323 (1982).
[43] D. Marion and K. Wüthrich, *Biochem. Biophys. Res. Commun.* **113,** 967 (1983).
[44] A. J. Shaka, P. B. Barker, and R. Freeman, *J. Magn. Reson.* **64,** 547 (1985).
[45] A. J. Shaka, J. Keeler, and R. Freeman, *J. Magn. Reson.* **53,** 313 (1983).

$R_S(S_z)$ Measurements. Figure 3A shows a sequence to measure the spin–lattice relaxation rates of the S spins, $R_S(S_z)$. The experiment is an S spin inversion recovery experiment inserted inside a 2D heteronuclear correlation spectrum. The S spin magnetization is inverted for the variable delay T after a refocused INEPT. The $\langle S_z \rangle$ magnetization relaxes along the z axis and is then tipped back to the transverse plane for frequency labeling and subsequent transfer back to proton with a reversed refocused INEPT. Two potential cross-relaxation pathways are present in the relaxation delay. First, the heteronuclear DD interaction will encourage cross-relaxation between the $\langle I_z \rangle$ and $\langle S_z \rangle$ at a rate $R_S(S_z \leftrightarrow I_z)$. Second, heteronuclear DD–CSA cross-correlation will allow cross-relaxation from $\langle S_z \rangle$ magnetization to $\langle 2I_zS_z \rangle$. This second form of cross-relaxation is substantially more serious than that originating from the heteronuclear DD interaction alone. Heteronuclear dipolar cross-relaxation rates, $R_S(S_z \leftrightarrow I_z)$, have been shown to be quite small relative to the $R_S(S_z)$ [typically $<5\%$ of $R_S(S_z)$]; this contribution becomes even smaller for larger proteins. The overall time course of $\langle S_z \rangle$ is summarized by the following differential equation:

$$\frac{d\langle S_z \rangle}{dt} = -R_S(S_z)\langle S_z - S_z^0 \rangle - R_{IS}(S_z \leftrightarrow I_z)\langle I_z - I_z^0 \rangle - R_{IS}(S_z \leftrightarrow 2I_zS_z)\langle 2I_zS_z \rangle \tag{4}$$

$R_{IS}(S_z \leftrightarrow I_z)$ is the cross-relaxation rate due to the heteronuclear DD interaction, and $R_{IS}(S_z \leftrightarrow 2I_zS_z)$ is the cross-relaxation rate due to DD–CSA cross-correlation. I_z^0 and S_z^0 are constants denoting the equilibrium Zeeman magnetizations of the I and S spins, respectively. (The equilibrium value of $2I_zS_z$ is 0.)

If the $\langle I_z \rangle$ and $\langle 2I_zS_z \rangle$ terms are kept constant or zero in Eq. (4), then the recovery of $\langle S_z \rangle$ is single exponential. The sequence of Fig. 3A achieves this by initially saturating the protons via two long pulses. The saturation is maintained throughout the relaxation delay, T, by a train of hard 90° pulses (typical separation is ~5 msec for 9 μsec 90° pulses). The proton saturation ensures that the two doublet components of $\langle S_z \rangle$ remain equal during the delay, and therefore cross-correlation effects are removed. Alternatively, proton broadband decoupling can be used to achieve the same aims. Note that the proton saturation employed during the relaxation delay forces the steady-state cross-peak intensity to a value determined by the heteronuclear NOE value. In the case of ^{15}N relaxation, this value is less than the equilibrium Zeeman magnetization owing to the negative value of the ^{15}N gyromagnetic ratio. For IS bonds with high internal mobility, the steady-state cross-peak intensity may even be negative.

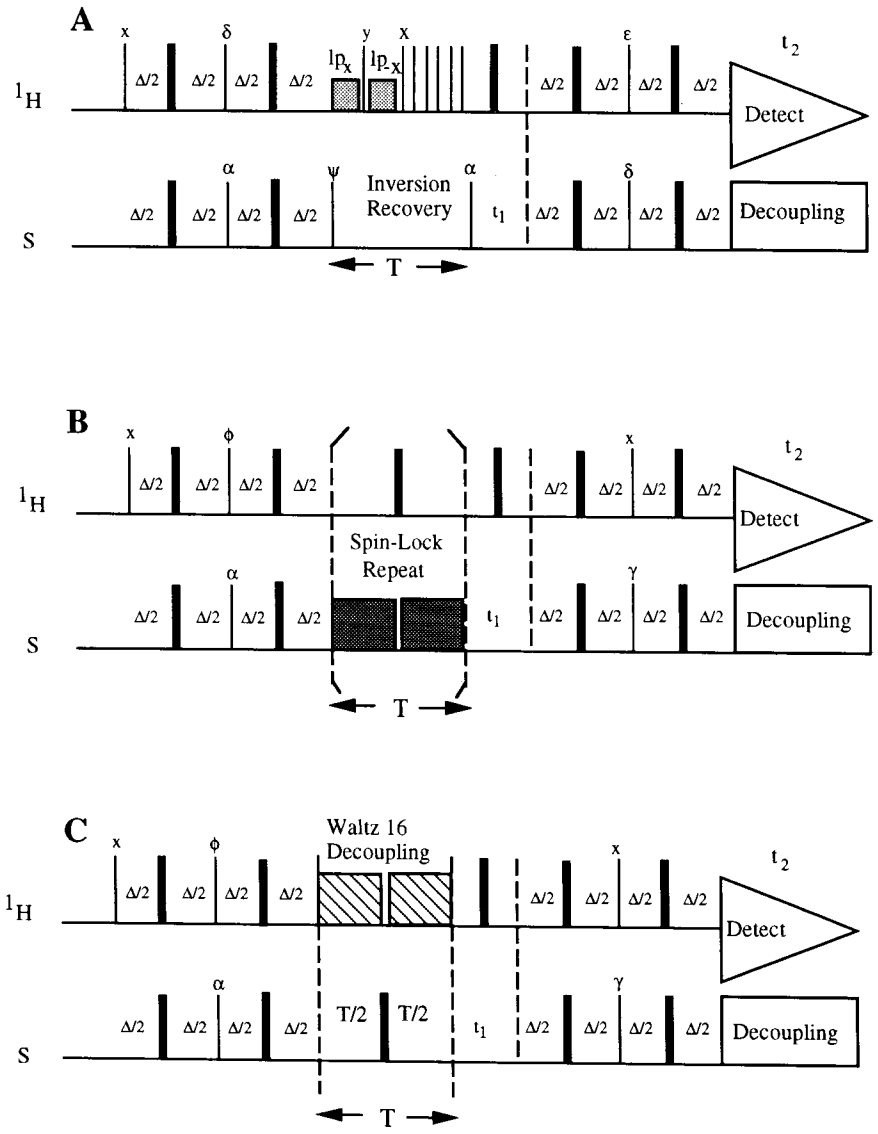

FIG. 3. Two-dimensional heteronuclear pulse sequences to obtain relaxation rates in *IS* spin systems. Proton pulses are given on the upper staffs, and heteronucleus (e.g., ^{15}N or $^{13}C^{\alpha}$) pulses are illustrated on the lower staffs. Thin and thick vertical bars represent 90° and 180° pulses, respectively. The delay Δ is typically set to a value slightly less than $1/(2J_{IS})$. The relaxation delay lasts for a variable length T. Basic eight-step phase cycles are indicated above the various 90° pulses using the following key: $\alpha = +x,-x$; $\beta = +y,-y$; $\gamma = 2(+x),2(-x)$; $\delta = 2(+y),2(-y)$; $\varepsilon = 4(+x),4(-x)$; and $\phi = 4(+y),4(-y)$. The receiver toggles as $+x,-x,-x,+x,-x,+x,+x,-x$ for sequences (A)–(H). Proton 180° pulses in the middle of the t_1 period are composites of the form 90_x–180_y–90_{-x}. For sequences using the spin lock, the TPPI phase modulation is done on the first 90° *S* pulse following the t_1 period. Otherwise, the TPPI phasing occurs before the t_1 period. (A) $R_S(S_z)$ pulse sequence. The minimum T length should allow for both long pulses (~1 msec each) to be executed prior to the train of 90° pulses. The 90° *S* pulse just prior to the T period is cycled

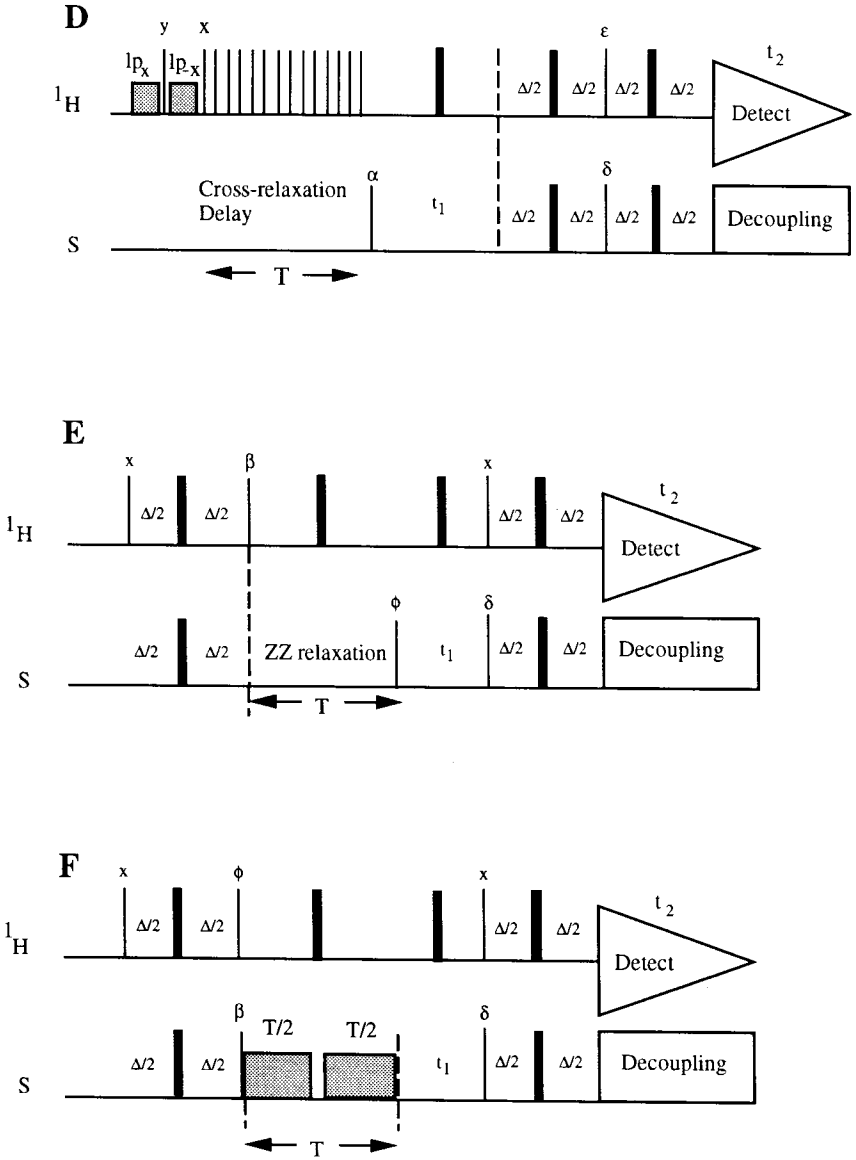

(continued)

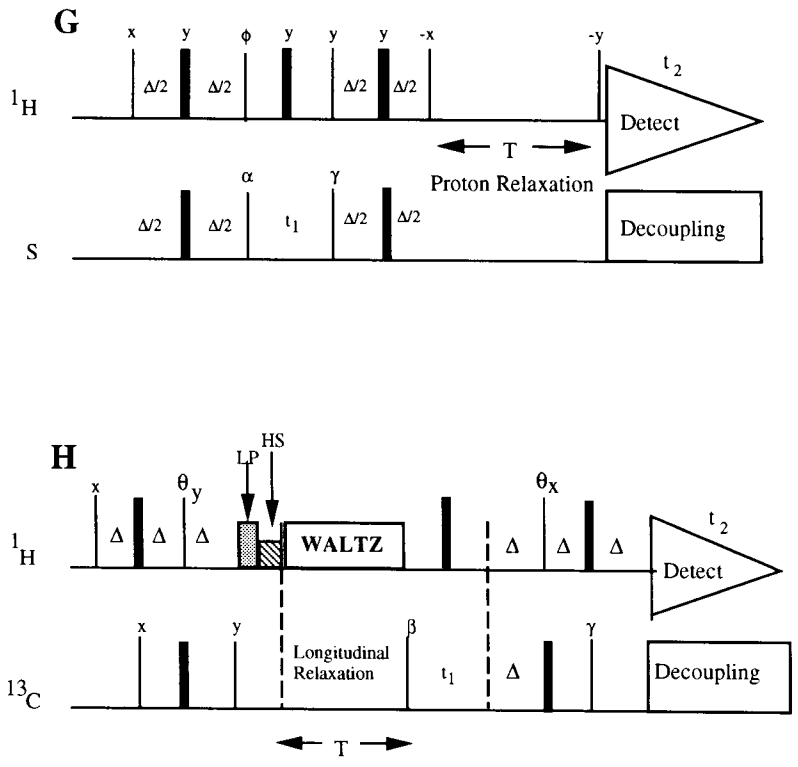

(continued)

as $\psi = +y, -y, -y, +y$. (B) $R_S(S_x)$ sequence. Typical spin-lock strengths are 2.5 to 3 kHz. The phase of the spin lock should be adjusted to compensate for possible phase shifts between low and high power outputs of the S amplifier. Hard proton 180° pulses are regularly interspersed after about 3 msec of spin locking. (C) Alternative $R_S(S_x)$ pulse sequence using proton broadband decoupling. (D) Heteronuclear cross-relaxation (NOE) sequence to measure $R_S(I_z \leftrightarrow S_z)$. (E) $R_{IS}(2I_zS_z)$ pulse sequence to measure the relaxation rate of longitudinal two-spin order, or zz-magnetization. (F) $R_{IS}(2I_zS_x)$ pulse sequence to measure the decay of antiphase coherence. The spin lock is the same as in sequence (B) but with only a single proton 180° hard pulse in the center of the relaxation delay. (G) S spin HSQC-NOESY sequence for measuring spin–lattice relaxation rates $R_I(I_z)$ for the I protons. (H) Two-dimensional pulse sequence to measure methyl ^{13}C longitudinal relaxation rates developed by Palmer *et al.* [A. G. Palmer III, P. E. Wright, and M. Rance, *Chem. Phys. Lett.* **185**, 41 (1991)]. The proton flip angle θ is set to 54.7° as explained in the text. LP indicates a long purge pulse, and HS refers to a homospoil period. The receiver phase toggles as $x, -x, -x, x$.

$R_S(S_x)$ Measurements. Figure 3B shows a sequence to measure the in-phase transverse relaxation rates, $R_S(S_x)$. After a refocused INEPT, transverse $\langle S_x \rangle$ magnetization is created. During the following relaxation delay period T, the $\langle S_x \rangle$ magnetization is subject to evolution under

both scalar coupling and relaxation. This is summarized by the rate equation

$$\frac{d\langle S_x \rangle}{dt} = -R_S(S_x)\langle S_x \rangle + \pi J_{IS}\langle 2I_zS_y \rangle - R_{IS}(S_x \leftrightarrow 2I_zS_x)\langle 2I_zS_x \rangle \quad (5)$$

In this rate equation, $R_S(S_x)$ is the relaxation rate of interest. The πJ_{IS} term describes the effect of the one-bond scalar IS coupling that causes oscillation between in-phase and antiphase S spin coherence. $R_{IS}(S_x \leftrightarrow 2I_zS_x)$ is the cross-relaxation rate between in-phase $\langle S_x \rangle$ and antiphase $\langle 2I_zS_x \rangle$ as a consequence of the cross-correlation between the heteronuclear DD and CSA interactions.

The desired evolution of $\langle S_x \rangle$ is a single-exponential decay determined purely by the natural relaxation rate $R_S(S_x)$. It is therefore necessary to kill the scalar coupling term and suppress the cross-relaxation. Use of a continuous wave spin lock along the x axis effectively kills the J_{IS} term since it prevents the oscillation between in-phase $\langle S_x \rangle$ coherence and antiphase $\langle 2I_zS_y \rangle$. The spin-locking segments are typically several milliseconds and approximately 2.5–3 kHz for ^{15}N on a 11.74 tesla magnet. Erroneously fast relaxation rates will be recorded if significant antiphase coherence develops, since what is actually being measured is the time-weighted average rate $R_{avg} = \cos^2(\pi J_{IS}T)R_S(S_{x,y}) + \sin^2(\pi J_{IS}T)R_{IS}(2I_zS_{x,y})$.[33] As stated, $\langle 2I_zS_{x,y} \rangle$ decays considerably faster than $\langle S_{x,y} \rangle$ owing to the strong effects of proton homonuclear DD interactions. If, instead of a spin lock, a Carr–Purcell Meiboom–Gill (CPMG) sequence is used,[46,47] then the spacing Δ in the CPMG echo $[\Delta\text{–}180°(S)\text{–}\Delta]$ should satisfy $2\pi J_{IS}\Delta \ll 1$.[33,34] For example, in the case of ^{15}N–^1H measurements, J_{NH} is around 90 Hz; therefore, values of Δ no greater than 0.5 msec are typically used. Cross-relaxation due to CSA–DD cross-correlation is suppressed by inserting proton 180° pulses between spin-locking segments as shown in Fig. 3B. The 180° pulses are typically under 20 μsec, so no significant in-phase and antiphase evolution of the S spins is expected to take place during this time. The apparent cross-relaxation from $\langle S_x \rangle$ to $\langle 2I_zS_x \rangle$ arises because the two doublet members of the transverse $\langle S_x \rangle$ magnetization relax at different rates. The proton 180° pulses periodically exchange the doublets, thereby averaging the intrinsic differences in relaxation rates. If the CPMG scheme is used, then proton 180° pulses are to be applied asynchronously from the ^{15}N 180° pulse in order to switch the double components; typically this involves flipping the protons after every even echo of the CPMG train.

[46] H. Y. Carr and E. M. Purcell, *Phys. Rev.* **94,** 630 (1954).
[47] S. Meiboom and D. Gill, *Rev. Sci. Instrum.* **29,** 688 (1958).

Rigorously, the sequence of Fig. 3B measures the decay of the x axis projection of S spin magnetization, which is undergoing nutation about the effective field in the rotating frame. Thus, in principle, the effects of both nutation and relaxation may enter into the time dependence of this component. In terms of the relaxation delay T, this dependence is given as

$$\langle S_x\rangle(T) = (\sin^2\beta)\exp[-R_S(S_{\rho z'})T] + (\cos^2\beta)\exp\left[\frac{R_S(S_{\rho x'}) + R_S(S_{\rho y'})}{2}\right]\left\{\cos(\Omega T) + 0.5[R_S(S_{\rho y'}) - R_S(S_{\rho x'})]\left(\frac{\sin\Omega T}{\Omega}\right)\right\} \quad (6)$$

In Eq. (6), β is the tip angle of the effective field relative to the laboratory z axis and becomes $\pi/2$ in the on-resonance limit. β is obtained from the S spin resonance offset, δ, and the applied radio frequency (rf) field strength f_1 through the relation $\tan(\beta) = f_1/\delta$. The angular nutation frequency about the effective field is given by $\omega_{\text{eff}} = 2\pi(\delta^2 + f_1^2)^{1/2}$. $R_S(S_{\rho z'})$ is the S spin relaxation time along the effective field axis denoted by z' and is the S spin $1/T_{1\rho'}$. $R_S(S_{\rho x'})$ and $R_S(S_{\rho y'})$ are the relaxation times along the tilted frame x' and y' axes in the doubly rotating, tilted frame. Note that these rates have contributions not only from the usual DD and CSA interactions, but also from the inevitable rf field inhomogeneity. Ω is given by $(\omega_{\text{eff}}^2 - \{0.5[R_S(S_{\rho x'}) - R_S(S_{\rho y'})]\}^2)^{1/2}$. Note that the second term in Eq. (6) becomes negligible for a spin lock applied near resonance owing to the $\cos^2\beta$ coefficient. Moreover, this term dies much more rapidly than the first term, owing to the rf inhomogeneity dependencies of the $R_S(S_{\rho x'})$ and $R_S(S_{\rho y'})$ rates. Thus, for tip angles near $\pi/2$, the experiment essentially measures $R_S(S_{\rho z'})$. Furthermore, if the spin-lock field does not affect the spectral densities, then $R_S(S_{\rho z'})$ is related to the laboratory rates $R_S(S_z)$ and $R_S(S_x)$ by

$$R_S(S_{\rho z'}) = (\sin^2\beta)R_S(S_x) + (\cos^2\beta)R_S(S_z) \quad (7)$$

Clearly, in the limit that $\beta \approx \pi/2$, $R_S(S_{\rho z'})$ is the same as $R_S(S_x)$.

A deceptively attractive alternative method to measure $R_S(S_x)$ involves the use of proton broadband decoupling during the relaxation delay. An example of such a sequence is shown in Fig. 3C. The relaxation delay now consists of a simple Hahn spin echo for the S spins, with WALTZ-16 decoupling applied on either side of the single S spin refocusing pulse. In principle, the decoupling scheme simultaneously kills the scalar coupling and cross-correlation effects. In our experience, such a sequence

yields relaxation rates similar to those obtained from the spin-locking sequence for most resonances and significantly larger rates for a few others. Kay *et al.* have reported similar effects, attributing them to the reduced decoupling performance of the proton rf scheme resulting from the presence of proton–proton scalar coupling.[34] In effect, the scalar coupling effects, πJ_{IS}, are not completely quenched, and therefore erroneously short $R_S(S_x)$ values may still be recorded.

The condition that a S spin spin lock does not affect the sampling of the spectral densities is given by the inequality $2\pi f_1\tau_{\text{corr}} \ll 1$, where τ_{corr} is a correlation time describing the slowest dynamic process responsible for relaxation in the IS spin system.[27] In effect, the rf field leaves the spin system unaffected on the time scale of the dynamic stochastic process. If the slowest process is simply molecular tumbling, then the inequality is certainly valid for proteins tumbling in solution which typically involve correlation times in the nanosecond regime. Correlation times closer to $1/f_1$ may arise if fast conformational exchange processes with lifetimes in the 100 μsec range are present, and, as a consequence, the spectral density will have an f_1 dependence. As demonstrated by Deverell *et al.*,[48] Brüschweiler *et al.*,[49] and Szyperski *et al.*,[50] this dependence can actually be exploited in experiments to characterize these fast exchange rates. One records a family of relaxation series using the pulse sequence of Fig. 3B at different field strengths. This results in a collection of relaxation rates for each cross-peak, distinguished by the various rf field strengths used. The extracted rates $R_S(S_{\rho z'})$ can be fitted to a functional form that expresses the observed $R_S(S_{\rho z'})$ as a sum of the usual DD and CSA effects and a new term describing exchange. The exchange term is assumed to have a Lorentzian dependence on the rf field strength f_1. Using these methods, Szyperski *et al.* have identified intramolecular exchange processes on the millisecond time scale for cysteines in ^{15}N-enriched BPTI.[50]

Heteronuclear NOE (Heteronuclear Cross-Relaxation Rate). The sequence to measure heteronuclear NOEs is shown in Fig. 3D. The experiment is essentially the $R_S(S_z)$ experiment without the first polarization transfer step. The sequence begins with a proton saturation scheme identical to the one used in the $R_S(S_z)$ experiment for a variable length T. Heteronuclear DD cross-relaxation concomitantly communicates the $\langle I_z\rangle$ perturbations to the heteronuclear $\langle S_z\rangle$ magnetization. The resulting $\langle S_z\rangle$

[48] C. Deverell, R. E. Morgan, and J. H. Strange, *Mol. Phys.* **18,** 553 (1970).
[49] R. Brüschweiler, M. Blackledge, and R. R. Ernst, *J. Biomol. NMR* **1,** 3 (1990).
[50] T. Szyperski, P. Luginbühl, G. Otting, P. Güntert, and K. Wüthrich, *J. Biol. NMR* **3,** 151 (1993).

magnetization is then read out using a single refocused reverse INEPT scheme. For $T = 0$, there is no saturation, and the S spin magnetization is simply the equilibrium Zeeman value $\langle S_z^0 \rangle$. For $T = \infty$, $\langle S_z \rangle$ reaches a steady-state intensity determined by the heteronuclear NOE value, as in the $R_S(S_z)$ experiment. The heteronuclear cross-relaxation rate, $R_S(I_z \leftrightarrow S_z)$, is extracted from combined NOE and $R_S(S_z)$ measurements using the familiar relationship given by Noggle and Schirmer[51]:

$$\eta = \frac{I_{sat} - I_{eq}}{I_{eq}} = \frac{\gamma_I}{\gamma_S} \frac{R_S(S_z \leftrightarrow I_z)}{R_S(S_z)} \tag{8}$$

In Eq. (8), η is the symbol denoting the NOE, and I_{sat} and I_{eq} are the cross-peak intensities at $T = \infty$ and $T = 0$, respectively. For ^{15}N–^{1}H systems, $I_{sat} < I_{eq}$ since γ_S is negative. Clearly, both I_{sat} and I_{eq} are needed for each IS resonance in order to extract the cross-relaxation rate from the NOE and $R_S(S_z)$. Thus, two families of 2D spectra must be recorded including an I_{sat} spectrum with T typically extending to several seconds, and an I_{eq} spectrum with $T = 0$. The steady-state condition can be verified by simply checking the 1D transformation of the first free induction decay (FID) for successively longer times T. Multiple spectra should be acquired for both I_{sat} and the I_{eq} spectra to estimate the precision in the resulting NOE and cross-relaxation rates.

It should be noted that the use of solvent presaturation can complicate measurements of the NOE in ^{15}N–^{1}H systems.[52,53] Specifically, the amide protons can experience some saturation even in the $T = 0$ experiment owing to rapid exchange with the saturated water protons. This effect is particularly pronounced if the recycle delay is too short. The amide protons remain partially saturated, and this is relayed to the amide ^{15}N, resulting in underestimation of the equilibrium Zeeman $\langle S_z \rangle$ magnetization. Underestimations of the Zeeman $\langle S_z \rangle$ magnetization produce erroneously small values of η, which in turn yield systematic underestimations of the heteronuclear cross-relaxation rates. Note that longer recuycle delays should also be anticipated since the experiment begins with the heteronuclear S spin polarization.

In summary, sufficiently long recycle delays should be employed to reduce such systematic errors in the NOE experiments. In principle, an alternative procedure to find the cross-relaxation rates involves recording a series of 2D spectra in which the T delay is systematically increased until the steady-state condition is reached. The initial slope of the cross-peak intensities versus T then gives the cross-relaxation rate. However, this method lacks precision if the steady-state peak intensities are quite close to the equilibrium Zeeman intensities [η almost 0 in Eq. (8)]. This is often the case for the more rigid IS spin pairs in larger proteins, and the result is an unsatisfactory dynamic range for the peak intensity, which renders estimation of an initial slope difficult.

[51] J. H. Noggle and R. E. Schirmer, "The Nuclear Overhauser Effect." Academic Press, New York, 1971.
[52] D. Neuhaus and C. P. M. van Mierlo, *J. Magn. Reson.* **100,** 221 (1992).
[53] N. J. Skelton, A. G. Palmer III, M. Akke, J. Kördel, M. Rance, and W. J. Chazin, *J. Magn. Reson. B* **102,** 253 (1993).

Relaxation Rates of $\langle 2I_zS_z \rangle$, $\langle 2I_zS_x \rangle$. The pulse sequences for measuring the autorelaxation rates of the heteronuclear longitudinal two-spin order $\langle 2I_zS_z \rangle$ and the S spin antiphase coherence $\langle 2I_zS_x \rangle$ are given in Fig. 3E,F, respectively. These spin orders can be visualized from the perspective of the S spins where the S doublet member with the proton spin up is polarized along $+z$ or $+x$, and the doublet member with proton spin down is polarized along $-z$ or $-x$. For the $R_{IS}(2I_zS_z)$ measurements, one first develops proton antiphase coherence $\langle 2I_xS_z \rangle$, which is then converted to $\langle 2I_zS_z \rangle$ after the second proton 90° pulse. Relaxation occurs for a time T, after which the remaining longitudinal two-spin spin order is frequency labeled and brought back to proton magnetization using a reversed INEPT. For the $R_{IS}(2I_zS_x)$ measurements, an initial INEPT creates antiphase S spin coherence, which is then spin locked for the relaxation delay T. As in the in-phase $R_S(S_x)$ measurements, the spin lock serves to prevent evolution under scalar coupling so that the relaxation rates of the antiphase coherence may be measured independently. The same considerations concerning spin-lock power and off-resonance effects are valid here as well. The readout sequence after the relaxation delay is essentially the same as in the $R_{IS}(2I_zS_z)$ experiment.

The decay of $\langle 2I_zS_z \rangle$ and $\langle 2I_zS_x \rangle$ during their relaxation delays are described by the following rate equations:

$$\frac{d\langle 2I_zS_z \rangle}{dt} = -R_{IS}(2I_zS_z)\langle 2I_zS_z \rangle - R_{IS}(2I_zS_z \leftrightarrow S_z)\langle S_z \rangle - \sum_i \sigma_L^i \langle 2A_z^iS_z \rangle \tag{9}$$

$$\frac{d\langle 2I_zS_x \rangle}{dt} = -R_{IS}(2I_zS_x)\langle 2I_zS_x \rangle - R_{IS}(2I_zS_x \leftrightarrow S_x)\langle S_x \rangle - \sum_i \sigma_L^i \langle 2A_z^iS_z \rangle \tag{10}$$

Equation (10) omits the evolution under heteronuclear scalar coupling, which has been assumed to be quenched as a result of the spin locking.

As stated, the rates $R_{IS}(2I_zS_z)$ and $R_{IS}(2I_zS_x)$ are significantly larger than the one-spin counterparts $R_S(S_z)$ and $R_S(S_x)$, owing to contributions from longitudinal proton relaxation. Additionally, Eqs. (9) and (10) show that proton DD cross-relaxation couples the *IS* spin system to other spin orders external to the *IS* spin system. With current high-field spectrometers, these cross-relaxation rates are essentially determined by $J_{IA^i}(0)$ [see Eqs. (3c) and (3d)]. These external spin orders are signified by $\langle 2A_z^iS_z\rangle$. The indexed sum i extends over all protons A^i close in space to the particular I proton under study. Even though the pulse sequences shown in Fig. 3E,F do not initially excite the $\langle 2A_z^iS_z\rangle$ spin orders, they may still arise from cross-relaxation. Therefore, these experiments are not yet completely satisfactory with regard to the suppression of these homonuclear cross-relaxation effects.

The decays of the two-operator spin orders also experience cross-relaxation to the in-phase counterparts as a consequence of the CSA–DD cross-correlation. Attempts to use trains of proton 180° pulses, as in the $R_S(S_x)$ pulse sequence of Fig. 3B, have not been successful. This is probably due to cumulative errors in the 180° proton pulses which tend to destroy the desired two-spin spin orders. Instead, a single proton 180° pulse is used in the center of the relaxation delay. This pulse performs one exchange of the two doublet components once, and therefore reduces but does not eliminate the CSA–DD cross-correlation effect. Fortunately, the cross-relaxation rate $R_{IS}(2I_zS_z \leftrightarrow S_z)$ is expected to be significantly smaller than the autorelaxation rates $R_{IS}(2I_zS_x)$ and $R_{IS}(2I_zS_z)$, since the latter rates have strong contributions from the aforementioned proton longitudinal relaxation. In effect, the more rapid proton relaxation in the autorelaxation rates quenches some of $\langle S_z\rangle$ or $\langle S_x\rangle$ that would otherwise have been built up in an isolated *IS* spin system. This fortuitous result is expected to become a better approximation for larger molecules since the proton longitudinal relaxation rates have essentially a $J_{IA^i}(0)$ dependence.

Measurements of Proton $\langle I_z\rangle$ Longitudinal Autorelaxation Rate. As shown above, proton relaxation has a significant influence on the auto- and cross-relaxation rates of the two-spin spin orders, such as $\langle 2I_zS_x\rangle$ and $\langle 2I_zS_z\rangle$. Thus, there is a motivation for having independent measurements of the longitudinal proton relaxation rate, $R_I(I_z)$. A pulse sequence for measuring $R_I(I_z)$ values is shown in Fig. 3G. The sequence is essentially a 2D heteronuclear single-quantum correlation (HSQC)-NOESY sequence with S spin shifts along ω_1 and proton shifts along ω_2.[54] The decay of the

[54] G. Wagner, *Prog. NMR Spectrosc.* **22,** 101 (1990).

direct *IS* cross-peaks with T is used to obtain proton longitudinal relaxation times. The rate equation for a given proton is

$$\frac{d\langle I_z - I_z^0\rangle}{dt} = -R_I(I_z)\langle I_z - I_z^0\rangle - R_{IS}(I_z \leftrightarrow S_z)\langle S_z - S_z^0\rangle - \sum_i \sigma_L^i \langle A_z^i - A_z^{i0}\rangle \tag{11}$$

The autorelaxation rate $R_I(I_z)$ contains the effects of not only the heteronuclear DD interaction, but also the purely proton–proton DD interaction. Each closely neighboring proton, A^i, contributes to the autorelaxation rate, resulting in the net ρ_L rate given in Eq. (3a). Additionally, many cross-relaxation pathways to various $\langle A_z^i\rangle$ become feasible.

Clearly, the proton relaxation has multiexponential behavior owing to cross-relaxation pathways σ_L^i facilitated by the homonuclear DD interactions. Additionally, there is cross-relaxation to the S spin owing to the heteronuclear DD interaction. However, the heteronuclear cross-relaxation is expected to be much smaller than the homonuclear cross-relaxation, since the latter has essentially a strong $J_{IA^i}(0)$ dependence as seen previously in Eq. (3c). The pulse sequence of Fig. 3G uses two techniques to help reduce the effects of the proton–proton cross-relaxation. First, the pulse phases are cycled such that only S-bound protons experience inversion during the relaxation delay; all protons not bound to S are flipped back to the $+z$ axis for all scans at the start of the relaxation delay. Second, the S-bound proton inversion is done only after the heteronuclear frequency labeling, and therefore the spins are inverted at different times according to the S spin chemical shift. Nonetheless, cross-relaxation with other protons will ensue in the manner of the classical transient NOE, irrespective of the initial conditions.[55] Selective saturation of all protons not bound to the S spin seems to be impracticable. However, in our studies of amide–proton longitudinal relaxation, a Taylor series analysis of the recovery with a linear coefficient gives the autorelaxation rate of the amide protons. In our experience, Taylor series expansions and exponential fits using only short mixing times yield very similar results. Other experimental remedies to cope with the multiexponential recovery are under investigation.

Multiple-Quantum Relaxation Measurements. In principle, multiple-quantum relaxation measurements can be extracted from the decays of doubly transverse spin orders, such as $\langle 2I_xS_x\rangle$. $\langle 2I_xS_x\rangle$ actually represents a sum of zero- and double-quantum coherences. Accordingly, the relaxation

[55] I. Solomon, *Phys. Rev.* **99** (No. 2), 559 (1955).

rate is an average of the rates for pure zero- and double-quantum coherence. If one considers only the heteronuclear DD interaction, heteronuclear multiple-quantum relaxation rates lack a $J(0)$ dependence for an isolated IS spin pair. However, a $J(0)$ dependence does enter via the CSA as seen in Table I. As stated, this dependence may be negligible in situations where the CSA contribution is small, as in the case of ^{13}C relaxation. Proton DD interactions introduce a strong homonuclear $J_{IA'}(0)$ dependence [see Eq. (3b)] through the ρ_T terms and facilitate more rapid decay of multiple-quantum coherence. Note that since the zero- and double-quantum coherences comprising spin orders such as $\langle 2I_xS_x \rangle$ relax at slightly different rates, a cross-relaxation process entailing other doubly transverse spin orders would seem inevitable. The possibility of such cross-relaxation pathways are under study. Unlike the single-quantum transverse relaxation measurements, heteronuclear coupling does not affect zero- or double-quantum evolution. However, measurements of the decay are expected to be complicated by passive homonuclear coupling to protons not bound to the S spin. Thus far, our initial experiments to measure multiple-quantum relaxation are not satisfactory with respect to this effect.

Example of ^{15}N–^1H Relaxation Measurement Procedures

A brief outline of the actual procedures involved in relaxation experiments is given. These procedures are based on experience in our laboratory with relaxation measurements of uniformly ^{15}N-enriched proteins including the proteinase inhibitor eglin c (70 residues), the Gal-4 DNA-binding domain (65 residues), and human dihydrofolate reductase (186 residues). Bruker AMX 300, 500, and 600 MHz spectrometers (Bruker Instruments, Inc. Billerica, MA) equipped with BSV-10 X-nucleus amplifiers were used for measurements.

Typically, one records a series of 8 to 10 2D heteronuclear spectra for a given relaxation rate. This includes at least one pair of spectra recorded with identical values for the relaxation delay. The set of duplicates are subsequently used in the postacquisition error analysis. Data set sizes are typically 1 MByte. These consist of 128 FIDs, each being 2048 complex points. Vertical (^{15}N) sweep widths typically vary between 1200 and 2000 Hz.

Suppression of the water line is a necessary burden in the ^{15}N relaxation studies. In situations where amide proton exchange is severely retarded (e.g., low pH), we have used presaturation with the proton carrier placed on the H_2O line. One can also place the proton carrier in the middle of the amides and momentarily jump the carrier frequency to the water resonance for presaturation. If the spectrometer hardware does not permit

carrier frequency jumping, then off-resonance DANTE methods can be used.[4] Solution conditions necessary to keep a protein stable may necessitate rapid amide proton exchange. In such cases, presaturation is ill-advised, and other means of water suppression such as the spin-lock purge pulses of Messerle *et al.* must be used.[56] In these methods, proton spin locks are applied at judicious locations in the polarization transfer schemes, such that the magnetization associated with the water (protons not bound to heterospins S) are rapidly rotated and spoiled by the applied rf inhomogeneity. The spin-locking pulses are typically about a millisecond long. Note that it is advisable to use several decibels (dB) of attenuation for these pulses, since their extensive use can shorten the lifetime of the proton transmitter. Also, because the phases of these purge pulses are crucial, potential phase offsets between the low and high power output modes of the proton transmitter need to be calibrated and compensated for.

The setup of pulse sequence parameters proceeds according to the basic setup of a heteronuclear correlation spectrum. On our machines, ^{15}N high power pulses are typically 35 μsec using 3 dB attenuation. For broadband decoupling in proton acquisition, ^{15}N pulses are about 150 μsec using 17 dB attenuation. Additional lower power ^{15}N pulses need to be calibrated for the spin-lock sequences of Fig. 3B,F. The strongest spin-lock powers we have used correspond to 3000 Hz, calculated from the inverse of a calibrated 360° pulse. Use of the proper rf phase is crucial for spin locking the S nuclei. Thus, one must calibrate and compensate for any relative phase offsets between the high and low power outputs of the X-nucleus transmitter. The time values for the relaxation delays should obviously be chosen in a manner that well characterizes the slope and steady-state value of the cross-peak intensity as a function of the relaxation delay. The longest relaxation delay required can be estimated simply by performing 1D versions (t_1 held fixed) of the 2D experiments and systematically increasing the relaxation delay until the spectrum intensities reach a steady-state value. For the $R_S(S_z)$ and NOE experiments (Fig. 3A,C), the steady-state value is determined via Eq. (8) and is often nonzero. For studies on eglin c, this amounted to a maximal delay of 3 sec. For the other experiments, the steady-state value is theoretically zero. In practice, inevitable pulse imperfections may result in nonzero steady-state values. A cautionary note is that the maximal delay possible for the spin-lock pulse sequences (Figs. 3B,F) may be limited by potential sample heating.

[56] B. Messerle, G. Wider, G. Otting, C. Weber, and K. Wüthrich, *J. Magn. Reson.* **85**, 608 (1989).

Once parameters have been optimized for a single 2D spectrum and the choice of relaxation delays have been made, a computer script can arrange for the series of 8–10 spectra to be acquired. In experiments with two polarization transfers, each 2D experiment takes about 1.7 hr using 16 scans per FID and a total recycle delay of 3 sec per scan. The NOE experiment requires typically longer recycle delays, since the experiment starts with ^{15}N Zeeman magnetization. The longer delay is also needed to allow for the possibility of the apparently longer ^{15}N T_1 caused by amide proton exchange with saturated water protons. It should be mentioned that spectra with equivalent signal-to-noise ratios can be obtained in half the acquisition time using the "sensitivity enhanced" versions of the 2D relaxation experiments of Palmer *et al.*[53,57] In these versions, both the cosine- and sine-modulated parts of the ^{15}N magnetization in the t_1 period are refocused and detected, in contrast to the pulse sequences shown in Fig. 3 which only refocus the cosine component. These methods required an additional pair of ^1H, ^{15}N 90° pulses and an INEPT-style refocusing stage in the second polarization transfer scheme before proton detection. The total data acquisition consists of acquiring two subdata sets, A and B, which differ in phase by 90° in both t_1 and t_2. The data sets are both added and subtracted to yield data sets ADD ($A + B$) and SUBTRACT ($A - B$). The ADD and SUBTRACT data are Fourier transformed and then summed to yield the final 2D spectra for relaxation analysis.

Fourier transformation of the series of 2D data typically produces spectra with 512 points in ω_1 (^{15}N) and 2048 points in ω_2 (^1H). We have used the software package FELIX2.06 (Hare Research, Seattle, WA) for all data processing. Sine-squared bells (60° shifted) are used for apodization and resolution enhancement. Note that negative ditches on the sides of the cross-peak caused by harshly shifted sine-bell apodization will damage cross-peak quantification. Resolution in ω_1 can be increased by using linear prediction methods. The virtues and disadvantages of using linear prediction in relaxation experiments have been discussed by Skelton *et al.*[53] In general, it appears that one can gain considerable accuracy for obtaining the relaxation rates of overlapped peaks in 2D spectra using linear prediction in the indirect dimension. However, the precision of the peak intensities, and therefore of the fitted rates, will be further compromised as the number of predicted points grows. The optimal balance between accuracy and precision must be chosen by the experimentalist.

Cross-peak intensities can be quantified by using volume integrals or by integration of cross-peak slices along one of the two frequency axes.

[57] A. G. Palmer III, J. Cavanagh, P. E. Wright, and M. Rance, *J. Magn. Reson.* **93,** 151 (1991).

We have employed both methods, using FELIX2.06 software (Hare Research) for volume integration and in-house software for the integration of slices parallel to ω_2. For cross-peaks that have no overlap, the fitted relaxation rates are essentially the same using either method of cross-peak quantification. For overlapped cross-peaks, we have preferred the integration of 1D slices; alternatively, linear prediction as mentioned above could be used. The final result of quantification are residue-specific ASCII files with relaxation delay and cross-peak integral as abscissa and ordinate, respectively.

To extract relaxation rates from the data, the files of relaxation delay versus cross-peak integral are fitted to single-exponential functions. For the longitudinal $R_S(S_z)$ experiment, the three-parameter functional form

$$I(T) = A \exp[-R_S(S_z)T] + B \tag{12}$$

is used. $I(T)$ is the cross-peak intensity as a function of the relaxation delay T. $(A + B)$ gives $I(0)$ and B yields $I_{\text{steady-state}}$. In the other pulse sequences, the theoretical steady-state value is zero. Therefore the two-parameter functional form

$$I(T) = A \exp[-R_{\text{spins}}(Q)] \tag{13}$$

can be used if the series does not entail long T delays such that a plateau in cross-peak intensity is reached. However, if sufficiently long T values are recorded for the experiments, the final steady-state value observed may not be zero due to instrument or pulse imperfections described above. In such cases, the previous functional form [Eq. (12)] is again used.

Equations (12) and (13) are fit to the experimental intensities using the Levenburg–Marquardt nonlinear least-squares algorithm.[58] The algorithm minimizes a chi-squared (χ^2) error function, which requires some knowledge of the uncertainties in the cross-peak intensities, or integrals. These uncertainties can be estimated from the fluctuations in cross-peak intensity between the aforementioned duplicate spectra. Of course, this assumes that the cross-peak uncertainties do not vary as a function of the relaxation delays. However, in our experience, larger fluctuations of peak intensity are seen in spectra that have the largest residual water signal. Similar observations have been reported elsewhere.[53] Thus, if uniform uncertainties are to be used for all relaxation delays, then estimates derived from duplicates of spectra with maximal residual water is the more cautious procedure. Uncertainties in the rates can be estimated using a Monte Carlo procedure.[7,14,34] In this procedure, an ensemble of hypothetical data sets are

[58] W. H. Press, B. P. Flannery, S. A. Teukolsky, and W. T. Vetterling, "Numerical Recipes in C—The Art of Scientific Computing." Cambridge Univ. Press, New York, 1988.

constructed from a Gaussian probability distribution that uses the observed peak intensities and their estimated uncertainties as the means and widths of the distribution. Each of the hypothetical data sets is fitted to a relaxation rate. The root mean square deviation (rmsd) of the ensemble of fitted relaxation rates yields an estimate of the uncertainty in the rate.

To translate the relaxation data into motional parameters, two general procedures can be used. In the first procedure, one uses a motional model to provide an analytical form for the spectral density function, $J_{\text{model}}(\omega)$. The dynamics parameters in $J_{\text{model}}(\omega)$ are adjusted in a least-squares fitting procedure to best reproduce the experimental data. Extremely popular $J_{\text{model}}(\omega)$ functions include those given by Lipari and Szabo and more recent extensions.[5,6,9] Fitting procedures for using the model-free approach are well described in the literature.[4–7,59] Using this approach, one can obtain order parameters and effective correlation times for the internal motions. The order parameters give an indication of the spatial freedom associated with the various internal motions. The order parameters can subsequently be interpreted in the context of more specific models of motion. Alternatively, direct access to the spectral density values are possible using a wider scope of relaxation measurements. It has been shown that if accurate values of the six rates namely, $R_S(S_z)$, $R_S(S_x)$, $R_{IS}(2I_zS_x)$, $R_{IS}(2I_zS_z)$, $R_S(I_z \leftrightarrow S_z)$, and $R_I(I_z)$, can be measured, then the following formulas can convert these rates to spectral density values:

$$J(0) = \frac{3}{4}\frac{1}{3d + c}\left\{-\frac{1}{2}R_S(S_z) + R_S(S_x) + R_{IS}(2I_zS_x) - \frac{1}{2}R_{IS}(2I_zS_z) - \frac{1}{2}R_I(I_z)\right\} \quad (14)$$

$$J(\omega_I - \omega_S) = \frac{1}{4}\frac{1}{d}\{R_S(S_z) - R_{IS}(2I_zS_z) + R_I(I_z) - 2R_S(I_z \leftrightarrow S_Z)\} \quad (15)$$

$$J(\omega_S) = \frac{1}{2}\frac{1}{3d + c}\{R_S(S_Z) + R_{IS}(2I_zS_z) - R_I(I_z)\} \quad (16)$$

$$J(\omega_I) = \frac{1}{12}\frac{1}{d}\{-R_S(S_z) + 2R_S(S_x) - 2R_{IS}(2I_zS_x) + R_{IS}(2I_zS_z) + R_I(I_z)\} \quad (17)$$

$$J(\omega_I + \omega_S) = \frac{1}{24}\frac{1}{d}\{R_S(S_z) - R_{IS}(2I_zS_z) + R_I(I_z) + 2R_S(I_z \leftrightarrow S_z)\} \quad (18)$$

[59] M. J. Dellwo and A. J. Wand, *J. Am. Chem. Soc.* **111,** 4571 (1989).

The constants d and c are listed in Table I, and typical values are listed in Table III. Of course, this strategy places harsher demands on the accuracy of the experiments involved. Uncertainties in model parameters or spectral density values can be estimated using Monte Carlo procedures analogous to those described above. Ensembles of synthetic relaxation rates are derived from a Gaussian distribution. Root mean square deviations of the motional parameters or spectral density values derived from the ensemble provide an estimate of the uncertainties.

Pulse Sequences for Relaxation Measurements in Non-*IS* Spin Systems

The majority of relaxation studies have focused on the ^{15}N–^1H and $^{13}C^{\alpha}$–^1H spin systems. These studies have provided insights into the dynamics of the protein backbone. Other potentially interesting dynamics can be probed by studying the relaxation properties of ^{13}C nuclei in protein side chains.[8,60] Another potentially interesting source of dynamics information can come from studying homonuclear relaxation rates using selective excitation schemes.

Sequences to Measure ^{13}C Relaxation of Methyl Groups

Accurate measurements of ^{13}C methyl T_1, T_2, and NOEs can be obtained using the methods developed by Palmer and Kay.[8,60,61] In these experiments, one must consider possible artifacts stemming from both coherent and incoherent evolution of an I_3S spin system. Figure 3H shows the pulse sequence used by Palmer *et al.* for measuring the ^{13}C methyl T_1 values.[60] This sequence uses the DEPT polarization transfer scheme. Special care must be taken such that only the desired spin orders are excited by the first DEPT. This means that the terminal 90° proton pulse of the first DEPT should be set to 54.7°. Similarly, the concluding reverse DEPT sequence should use the same final flip angle to select only the desired one-spin spin order $\langle S_z \rangle$ in preparation for proton detection. Measurement of methyl ^{13}C T_2 values involves omitting the second ^{13}C 90° pulse and inserting a modified CPMG sequence for the ^{13}C spins into the relaxation delay T. The modified CPMG sequence is the same as discussed in the previous section on the $R_S(S_x)$ measurements and involves inverting the protons at every even echo of the CPMG.[61] ^{13}C–^1H NOE values can be obtained by deleting the initial DEPT transfer of the T_1 sequence and simply beginning with the proton saturation.[61]

[60] A. G. Palmer III, P. E. Wright, and M. Rance, *Chem. Phys. Lett.* **185,** 41 (1991).

[61] A. G. Palmer III, R. A. Hochstrasser, D. P. Millar, M. Rance, and P. E. Wright, *J. Am. Chem. Soc.* **115,** 6333 (1992).

Pulse sequences used by Kay *et al.* are based on the INEPT scheme, in which the delays are adjusted according to the magic angle.[8] An initial proton saturation develops a heteronuclear $^{13}C-^{1}H$ NOE in order to boost the initial ^{13}C magnetization, instead of a polarization transfer pulse scheme. In these experiments, cross-relaxation effects will be present during the relaxation delay, T, which are due to cross-correlations between the DD interactions of different $^{13}C-H$ pairs in the methyl group. Thus, the data analysis is *a priori* more complicated since the decays are not expected to follow single-exponential curves. The results of the experiments yield information about the dynamics of the methyl symmetry axis and about the internal motions of the $^{13}C-^{1}H$ bonds attached to it.

Proton Cross-Relaxation Rates

Proton cross-relaxation rates are sensitive to the dynamics of proton spin pairs. As a result, one can monitor the dynamics of internuclear vectors that are not limited to specific chemical bonds. This may allow a better description of "long-range" dynamic processes. In a theoretical study, Brüschweiler *et al.* have proposed procedures to extract intramolecular dynamics information from a combination of NOESY and ROESY cross-relaxation rates.[62] In particular, NOE/ROE ratios can reveal dynamics information, provided that the correlation time for the intramolecular dynamics is comparable to the correlation time for molecular tumbling and that the NOE and ROE cross-relaxation rates maintain a significant dependence on $J(2\omega_I)$ [see Eqs. (3c) and (3d)].

A principal complication with proton relaxation is the network of auto- and cross-relaxation pathways that have to be considered *a priori* when trying to analyze the data. However, Burghardt *et al.* have developed methods whereby the dynamics of select proton pairs can be studied.[63] One begins with either equilibrium Zeeman magnetization $I_{1z} + I_{2z}$ or their difference $I_{1z} - I_{2z}$. The latter can be achieved by inversion of one of the resonances using a selective 180° pulse. Application of a selective pulse train $(360°_{x}\text{–}360°_{-x})$ with the carrier midway between the resonances Ω_{I1} and Ω_{I2} and modulated by $\cos[(\Omega_{I1} - \Omega_{I2})t]$ causes synchronous on-resonance nutation of spins I_1 and I_2. The selective nutation has the effect of isolating the proton pair from relaxation and coupling interactions with other spins in the molecule. As a result, the observables, $\langle I_{1z} + I_{2z}\rangle$ and

[62] R. Brüschweiler, B. Roux, M. Blackledge, C. Griesinger, M. Karplus, and R. R. Ernst, *J. Am. Chem. Soc.* **114,** 2289 (1992).

[63] I. Burghardt, R. Konrat, B. Boulat, S. J. F. Vincent, and G. Bodenhausen, *J. Chem. Phys.* **98,** 1721 (1993).

$\langle I_{1z} - I_{2z}\rangle$, decay as single exponentials. Differences in their relaxation rates are a direct manifestation of the homonuclear dipolar cross-relaxation rates between the two protons. Thus, this technique allows accurate measurements of homonuclear cross-relaxation rates for select proton pairs.

Concluding Remarks and Future Directions

Thus far, most of the relaxation measurements of proteins has focused on the ^{15}N nucleus. This has provided insight into the general flexibility of the protein backbone. For proteins that have the benefit of ^{15}N enrichment to aid conformational analyses, a set of complementary backbone dynamics experiments will become routine.

Future relaxation studies will undoubtedly focus on the dynamics of other parts of the protein structure and different time scales of motion. For example, increased ^{13}C relaxation studies should permit a more detailed picture of side-chain dynamics. However, further pulse sequence development may be needed to ensure accurate relaxation measurements in these more complicated spin systems. This has already been evident in the case of methyl carbon experiments. ^{13}C measurements in uniformly enriched proteins must also reckon with the problem of $^{13}C-^{13}C$ homonuclear couplings affecting the data. Specifically, accurate ^{13}C T_2 values require a method that can measure homonuclear T_2 values while simultaneously suppressing coherence transfer in the rotating frame. Alternatively, selective or partial carbon labeling may be a solution.

The increased sophistication of selective excitation and coherence transfer techniques for proton relaxation measurements will allow the dynamics of specific proton pairs to be studied; thus, long-range dynamic processes can be explored. Such techniques may be quite informative for studying the dynamics at the interface of a biomolecular complex. Exploitation of cross-correlated mediated relaxation will also provide information about the coupling of motions within the protein. Finally, lower frequency motions in proteins (e.g., microsecond time scales) will be examined more closely through relaxation measurements in the presence of spin-locking fields. Indeed, relaxation studies have strengthened the view that protein motions are likely to show more variability in the lower frequencies well below the 400 MHz range.[14] Exploration of lower frequency regimes may yield motions that are more collective. The end goal of all of these research directions is to gain a clearer picture of protein dynamics using NMR and, eventually, to understand their relevance to biological function.

Acknowledgments

This work was supported by the National Science Foundation (Grant DMB-9007878), the National Institutes of Health (Grant GM38608) and the Keck Foundation. We thank Dr. Dennis Hare for providing the software package FELIX2.06. We are grateful to Prof. Jean-François Lefèvre, Mr. Kwaku Dayie, and Dr. Johan Kördel for fruitful discussions. We also thank Prof. Geoffrey Bodenhausen and Prof. Arthur Palmer for providing manuscripts prior to publication.

[21] Nuclear Magnetic Resonance Measurements of Slow Conformational Dynamics in Macromolecules

By ANDREW N. LANE and JEAN-FRANÇOIS LEFÈVRE

Introduction

Dynamic processes occur on a wide variety of time scales in macromolecules, from rapid fluctuations in torsion angles to activated conformational transitions involving collective motions of a large number of atoms. Fast motions characterized by frequencies of the order of gigahertz (GHz) are accessible to molecular dynamics calculations[1,2] and can be detected by several physical methods including fluorescence depolarization[3] and nuclear magnetic resonance (NMR) relaxation.[4–8] Much slower motions involving concerted movements of groups of atoms are often involved in enzyme catalysis; conformational rearrangements of enzyme–substrate complexes during the catalytic cycle occur typically in the range of milliseconds to microseconds and can be the limiting factor in the overall turnover.[9,10]

[1] S. Swaminathan, G. Ravishanker, and D. L. Beveridge, *J. Am. Chem. Soc.* **113,** 5027 (1991).
[2] D. A. Pearlman and P. A. Kollman, *J. Mol. Biol.* **220,** 457 (1991).
[3] S. Barkley and B. Zimm, *J. Chem. Phys.* **70,** 2991 (1979).
[4] G. M. Clore, A. Szabo, A. Bax, L. E. Kay, P. C. Driscoll, and A. M. Gronenborn, *J. Am. Chem. Soc.* **112,** 4989 (1990).
[5] G. M. Clore, P. C. Driscoll, P. T. Wingfield, and A. M. Gronenborn, *Biochemistry* **29,** 7387 (1990).
[6] C. M. Dobson, E. T. Olejnicjak, F. M. Poulsen, and R. G. Ratcliffe, *J. Magn. Reson.* **48,** 97 (1982).
[7] T. M. G. Koning, R. Boelens, G. A. van der Marel, J. H. van Boom, and R. Kaptein, *Biochemistry* **30,** 3787 (1991).
[8] J. Kördel, N. J. Skelton, M. Akke, A. G. Palmer, and W. J. Chazin, *Biochemistry* **31,** 4856 (1992).
[9] A. Fersht, "Enzyme Structure and Mechanism." Freeman, New York, 1985.
[10] H. Gutfreund, *Biophys. Chem.* **26,** 117 (1987).

Multiple conformations that interconvert on the millisecond to microsecond time scale may be common in macromolecules under physiological conditions.[5,11–19] It is therefore important to characterize these slower conformational transitions in greater detail when attempting to describe the functional properties of macromolecules such as enzymes or receptors. Further, conformational heterogeneity may have significant consequences for the description of a structure based on NMR data.[20–22] Although molecular dynamics simulations can shed light on the effects of subnanosecond motions on NMR observables such as coupling constants and cross-relaxation rate constants,[1,2,23] they cannot be used to determine the influence of much slower motions on the NMR parameters. However, low frequency motions may be associated with rather large conformational fluctuations, such as interconversion of rotameric states, which certainly affects three-bond coupling constants[23] and may result in significant changes in mean interproton distances, and therefore nuclear Overhauser effect (NOE) intensities. Whereas this may have only a relatively small effect on the structures calculated using large numbers of NOE constraints,[5,14] refinements based on 'back-calculations' may be compromised by the averaging unless specific and appropriate motional models are directly incorporated into the refinement procedures.[7,24] Any refinement procedure that imposes a unique conformation as a constraint on the data under these circumstances must lead to a virtual structure of questionable relevance.[25]

[11] D. Ehrenstein and G. U. Nienhaus, *Proc. Natl. Acad. Sci. U.S.A.* **89,** 9681 (1992).
[12] Y. Kim and J. H. Prestegard, *Proteins* **8,** 377 (1990).
[13] P. A. Evans, C. M. Dobson, R. A. Kautz, G. Hatfull, and R. O. Fox, *Nature (London)* **329,** 266 (1987).
[14] P. C. Driscoll, A. M. Gronenborn, P. T. Wingfield, and G. M. Clore, *Biochemistry* **29,** 4668 (1990).
[15] M. S. Searle, M. J. Forster, B. Birdsall, G. C. K. Roberts, J. Feeney, H. T. A. Cheung, I. Kompis, and A. J. Geddis, *Proc. Natl. Acad. Soc. U.S.A.* **85,** 3787 (1988).
[16] J.-L. Leroy, E. Charretier, M. Kochoyan, and M. Guéron, *Biochemistry* **27,** 8894 (1988).
[17] X. Gao and D. J. Patel, *J. Am. Chem. Soc.* **110,** 5178 (1988).
[18] C. Carbonnaux, G. A. van der Marel, J. H. van Boom, W. Guschlbauer, and G. V. Fazakerley, *Biochemistry* **30,** 5449 (1991).
[19] A. N. Lane, T. C. Jenkins, D. J. S. Brown, and T. Brown, *Biochem. J.* **279,** 269 (1991).
[20] J. Fejzo, A. M. Krezel, W. M. Westler, S. Macura, and J. Markley, *Biochemistry* **30,** 3808 (1991).
[21] A. E. Torda, R. M. Scheek, and W. F. van Gunsteren, *J. Mol. Biol.* **214,** 223 (1990).
[22] T. M. G. Koning, R. Boelens, and R. Kaptein, *J. Magn. Reson.* **90,** 111 (1990).
[23] J. C. Hoch, C. M. Dobson, and M. Karplus, *Biochemistry* **24,** 3831 (1985).
[24] B. A. Borgias, M. Gochin, D. J. Kerwood, and T. L. James, *Prog. NMR Spectrosc.* **22,** 83 (1990).
[25] O. Jardetzky, *Biochim. Biophys. Acta* **612,** 227 (1980).